Growth and characterization of superconducting $YBa_2Cu_3O_{7-\delta}$-$BaZrO_3$ thin films.

Author: Núria Alcalde Herraiz*
Advisors: Albert Queraltó[1], Teresa Puig[1] and Arantxa Fraile Rodríguez[2].
[1]*Institut de Ciència de Materials de Barcelona, ICMAB-CSIC, Bellaterra, Spain.*
[2]*Facultat de Física, Universitat de Barcelona, Diagonal 645, 08028 Barcelona, Spain.*

Abstract: The future fabrication of high-temperature-superconductor-based coated conductors depends on the current research of thin films' growth processes, especially in developing low cost, scalable and industrially processing methods. A new transient liquid assisted growth method is explored through the growth of $YBa_2Cu_3O_x - BaZrO_3$ and $YBa_2Cu_3O_x$thin films. The characterization of spin-coating deposed thin films verified *c*-axis epitaxy, although the presence of secondary phases within the film were also confirmed. $BaZrO_3$ nanoparticles proved to be useful to enhance density superconducting properties at high fields, furthermore a 1.77 MA cm^{-2} current density was achieved for $YBa_2Cu_3O_x - BaZrO_3$ films at 5 K, whereas for lesser fields $YBa_2Cu_3O_x$ current density was up to 19.94 MA cm^{-2} also at 5 K. Critical temperatures of (89.2 ± 0.6)K and (90.6 ± 0.4) K were obtained for the films, respectively. First steps towards a new combinational chemistry approach for the inkjet printed samples were also performed.

I. INTRODUCTION

Multilayered Coated Conductors (CCs) overcame the manufacturing long, robust and flexible conductors challenges of High Temperature Superconductors (HTS) for their use in large scale energy applications and powerful magnets [1]. However, their large production costs are a limitation for a wide market implementation [1]. Consequently, the current research is focused on exploring and enhancing high growth rates processes of HTS layers and their properties.

The core of this research is $YBa_2Cu_3O_{7-\delta}$ (YBCO), a ceramic superconductor with a critical temperature (T_C) of 92 K that exhibits the most favourable performance for both low and high magnetic fields, as well as high temperature applications [1]. YBCO crystalline structure is based on a triple perovskite ABO_3. Particularly, a central $YCuO_2$ cube with two adjacent $BaCuO_3$ cubes along *c*-direction. In the former, *Y* takes the central position and is stacked by CuO_2 planes through which the supercurrent flows. The CuO_2 superconducting planes are separated by normal blocks which contain metallic *Cu-O* chains, that define the actual charge carrier density of the CuO_2 planes by charge transfer [2]. The structure anisotropy affects both normal and superconductor states. In the latter, current density along the *ab* planes is orders of magnitude higher than the one along the *c*-axis [3]. Thus, *c*-axis epitaxial growth is required to achieve maximum performance.

As a type II superconductor, YBCO mixed state is dominated by the presence of vortices [4]. Hence, to not truncate the HTS non-dissipation current flow at high magnetic fields, a vortex pinning mechanism is required. Studies revealed that nanocomposites with non-superconducting secondary nano-phases (nanorods, nanoparticles), are the most effective vortex pinning centres [4], [5]. When using Chemical Solution Deposition (CSD) as a preparation method, the pinning mechanism is mostly dominated by the presence of highly strained nano-scale areas, nanostrain, induced by the nanoparticles. Artificial pinning centers (APC) such as $BaMO_3$ (M = *Zr, Hf*) have become among the cost effective secondary nano-phases in nanocomposites [4].

Therefore, the overall objective to achieve CCs manufacturing is to find a scalable deposition method with a high growth rate. Until now, CSD by spin-coating has been used only at laboratory scale with slow growth rates ($1\ nm\ s^{-1}$) for the traditional CSD-trifluoroacetate route [6]. A compatible CSD of YBCO pristine films is ink-jet printing (IJP) [7], [8]. Moreover, recently, a novel transient liquid assisted growth (TLAG) method has been reported, enabling to reach ultrafast growth rates ($100\ nm\ s^{-1}$) with high critical current densities ($5\ \ MA\ cm^{-2}$ at *77K*) compatible with CSD, IJP and nanocomposites growth [6], though the latter's preparation is still a challenge for the growth routes.

The aim of this TFG research is to explore the new TLAG route using different YBCO-BMO (M=Zr) sample growth conditions, growth temperature and composition, and correlate them with their superconducting properties. Besides, a new approach for YBCO-BZO IJP thin films has been explored.

II. SAMPLE PREPARATION

Epitaxial YBCO and YBCO-BZO nanocomposite thin films were grown on single-crystalline (100) $SrTiO_3$ (STO) 5x5 mm^2 substrates. Samples were prepared from a metalorganic precursor solution with stoichiometry $YBa_2Cu_{4.66}O_x$ as epitaxial growth conditions are more likely to be reached with an initial Cu excess composition [9]. The solution characteristics were adapted to each deposition technique: spin-coating and IJP.

For the former, *Y*, *Ba* and *Cu* anhydrous acetates were dissolved in propionic acid for four hours at 50ºC, then anhydrous methanol was added to reach a *0.7M-1.5M* concentration depending on the BZO solution proportion and concentration. Spin-coated samples, deposited at 6000 r.p.m for 2 minutes, were prepared in a clean-room environment with *0%, 6%, 12%* or *24%* mol BZO proportion with a final YBCO concentration of *0.7M*. To obtain the colloidal solution, a forehanded BZO solution was added to the YBCO one. Thin film thickness was also varied, and more than one layer was deposited to enable the comparison between different films.

IJP follows a new combinational chemistry approach, as the deposited solution was not a colloidal one. Instead, two different solutions were prepared: one of YBCO and a second of BZO. Then they were printed on drop-on-demand to form the final layer. Therefore, the film thickness is not only controlled by the solution concentration, but also by the drop

* Electronic address: nurialhe@gmail.com

volume ($150 - 180\ pL$) and drop spacings along x and y directions. This approach brings a very interesting opportunity since the amount of nanoparticles in the film is not limited by the stability of the nanoparticles in the YBCO solution, and larger nanoparticle concentrations can be obtained [10].

Prior to the TLAG growth process, pyrolysis was carried out for all the samples. The temperature was increased at 5 $ºC\ s^{-1}$ heating rate till 240ºC and then at 3 $ºC\ s^{-1}$ until the final temperature. Single-layered wet films were pyrolyzed at 500*ºC* for 5 minutes, while bilayered and trilayered samples were pyrolized at 300ºC and 500ºC also, respectively, both with a five minutes dwell time. The thermal process was made with a humidified gas with $P_{H_2O} = 23$ mbar achieved through an oxygen flow of 0.12 L min^{-1} .

Subsequently, both YBCO and YBCO-BZO thin films were grown in a tubular furnace following the so-called TLAG's pressure route [6]. Thus, temperature and pressure conditions are selected so *Ba-Cu-O* prefers to rapidly form a transient liquid coexisting with Y_2O_3 nanoparticles. The desired temperature (T_{growth}) is achieved with heating ramps of 15 $ºC\ s^{-1}$ at 10^{-5} bar constant pressure (P_{total}=PO_2). Next, after a 2 minutes dwell time at T_{growth}, a pressure jump is made to 10^{-3} bar. At these conditions, the transient liquid forms and Y_2O_3 nanoparticles dissolve in it. A diffusion process of *Y* atoms occurs towards the substrate interface and heterogeneous nucleation is achieved at the lattice-matched substrate/interface. Hence, high growth rates of about 100 nm/s are obtained, as confirmed by in-situ XRD Synchrotron radiation experiments [4], due to a faster atomic diffusion in the liquid state than in solid states. High growth temperatures are required for promoting *c*-axis epitaxy [9]. In this work, different T_{growth} were used: 827ºC, 837ºC, 838ºC, 843ºC and 850ºC.

Following TLAG growth process to form $YBa_2Cu_3O_6$, an oxygenation process is undertaken to bring the insulating tetragonal $YBa_2Cu_3O_6$ phase to the orthorhombic $YBa_2Cu_3O_{7-\delta}$ superconducting one. The oxygenation process was carried out in a tubular furnace at 450ºC for approximately 210 minutes with an oxygen flow of 0.5 L/min.

III. YBCO and YBCO-BZO NANOCOMPOSITE CHARACTERIZATION

A total of fifteen thin films were prepared through spin-coating. One single-layered YBCO pristine film at 830ºC and five bilayer pristine films at different growth temperatures: 827ºC, 837ºC, 838ºC, 843ºC, 850ºC. Then nine YBCO-BZO with different layers. Two films (one single layer and one bilayer) with 6% mol BZO grown at 832ºC. Four films with 12% mol BZO: three grown at 832ºC, two one-layered, one two-layered and one three layered. Three trilayer films with 24% mol BZO grown at 827ºC, 832ºC, 837ºC.

In all cases, structural and physical characterization of the samples was done to compare both sample growth temperature and composition with their superconducting properties.

A. Morphological and structural characterization

Thin films surfaces, already electrically conducting after oxygenation, were inspected by Scanning Electron Microscopy (SEM) at ICMAB in order to identify surface morphology inhomogeneities, grain orientations and precipitates on the surface morphology. Images were taken on a field emission FEI Quanta 200 FEG SEM of FEI CompanyTM under high vacuum conditions with an acceleration voltage of ~15kV.

Qualitative epitaxial and random fractions analysis of grown films were made with a General Detector Diffraction System (GADDS) 2D detector, integrated in a Bruker D8 diffractometer. It operates with CuK_α radiation (λ = 1.5418 Å) and 12 cm of detector-sample distance**.** Two type of measurements were performed: θ – 2θ scans and ϕ-scans/pole figures. A further microstructural analysis of the samples was made through high-resolution XRD (HRXRD) performed with Discover D8 Bruker diffractometer (X-ray energy = 8.049 keV) equipped with a Lynxeye XE energy dispersive 1D detector, using a Bragg-Brentano configuration. Both XRD measurements were made at ICMAB by XRD service technicians. These analyses were performed to obtain information about the lattice disorder through quantitative rocking (or ω scan), nanostrain and epitaxial fraction calculations. The former offers information about film crystalline quality related with the full width at half maximum (FWHM) of a specific peak, YBCO (005), higher when the peak is narrower. Nanostrain was calculated through semiquantitative Williamson-Hall plots as non-uniform strain produces a broadening of the diffraction peak, and stress is a key mechanism for vortex pinning [4]. The epitaxial fraction is referred to the percentage of *c*-axis oriented grains with respect to the YBCO orientation. Following [9] approach, the epitaxial fraction was determined using the integrated areas of (005)YBCO, heterogeneous nucleation, (103)YBCO, homogeneous nucleation, and secondary phases:

$$\Gamma_{epitaxy} = \frac{(005)\ \text{YBCO}}{(005)\text{YBCO} + (103)\text{YBCO} + \text{Secondary phases}} \quad (1)$$

B. Physical characterization

Characterizations on the superconducting properties can be performed from a superconducting quantum interference device (SQUID) and from electrical transport measurements. SQUID measurements determined the critical current density (J_c) of the thin films. Thus, the sample is cooled down without a magnetic field applied to it (Zero Field Cooling conditions) to 5K and/or 77K. Then, a hysteretic magnetization curve is obtained measuring the magnetization (m) values when a magnetic field parallel to YBCO *c*-axis is increases up to 7T and then decreases. The J_c is obtained following the Bean model [11] for a squared shape thin disk:

$$J_c = \frac{3\,m}{a^3 t} \quad (2)$$

Where *a* is the lateral sample dimension and *t* is the sample thickness. Electric transport measurements to establish critical temperature (T_C) were performed using a Physical Properties Measurements System (PPMS). Van der Pauw method was employed to avoid the contact resistivity[12]. Both physical measurements were performed at ICMAB by the technicians.

IV. YBCO and YBCO-BZO NANOCOMPOSITE RESULTS

A. Morphology and structure

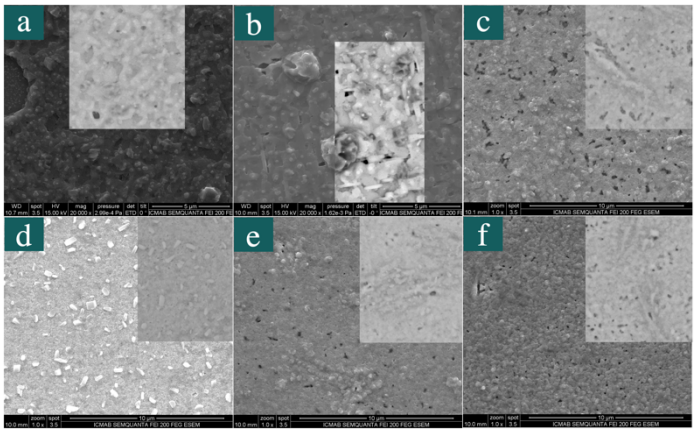

FIG. 1: SE SEM with insets of BSE SEM measurements of six TLAG films. a) Pristine film grown at 827ºC. b) Pristine film grown at 827ºC c) YBCO-BZO 6%mol grown at 832ºC d) YBCO-BZO 12%mol grown at 832ºC. e) YBCO-BZO 24%mol grown at 832ºC. f) YBCO-BZO 24%mol grown at 827ºC.

SEM measurement of a T_{growth} 838ºC pristine YBCO Fig.1(b) shows that the initial Cu excess in the proposed stoichiometry, $YBa_2Cu_{4.66}O_x$, leads to the presence of *CuO* precipitates on the surface, as *CuO* appear brighter in the SE mode due to their higher thickness and darker in the BSE because of its lower atomic number. The presence of the precipitates on the film surface does not interfere with the superconductivity properties. Nevertheless, the presence of *CuO* precipitates is not confirmed neither for T_{growth}= 827ºC pristine YBCO (Fig.1(a)), T_{growth}=832ºC YBCO-BZO(6%) (Fig.1(c)), T_{growth}=832ºC YBCO-BZO(24%) (Fig.1(e)), nor for T_{growth} =827ºC YBCO-BZO(24%) (Fig.1(f)). For T_{growth}=832ºC YBCO-BZO(12%) (Fig.1(d)), a precipitate on the surface is observed though it cannot be identified as *CuO* excess.

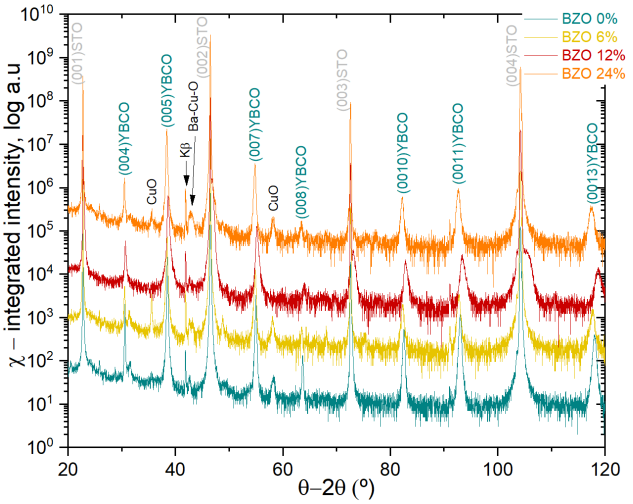

FIG. 2: X-Ray $\theta - 2\theta$ analysis (X-ray energy = 8.049 keV) of TLAG samples. Different nanoparticles content (up to 24% mol) and growth temperature (T_{growth} = 832ºC, for 6% and 12% mol BZO, and T_{growth} = 827ºC, 0% and 24% mol BZO) and are evaluated. Thus, (00l) peaks of YBCO and secondary phases of *CuO* and *Ba-Cu-O* and a K_β belonging to the HDXRD source.

Furthermore, the presence of *CuO* as well as *Ba-Cu-O* secondary phases were confirmed by HRXRD, as shown in Fig.2. Trapped *CuO* and *Ba-Cu-O* liquid could be responsible for the observed decrease in the electrical performance. As Fig.1(b) would suggest, this drawback should be corrected by lowering growth temperatures. This result is in agreement with literature as Volmer-Weber is suitable to be the nucleation model for YBCO [9], where the density of nuclei is inversely proportional to the growth temperature [13]. Thus, the higher the nuclei density, achieved at low temperatures, the lesser liquid between grain boundaries. However, lowering too much the growth temperature triggers the growth of a/b-oriented grains instead of the *c*-axis [9]. Thus, a further secondary phases analysis could be performed in an extended research.

Despite of the fact that Fig.2 shows a *c*-axis growth preference for the prepared samples, notice that the (001)YBCO is not a determinant factor to qualify the epitaxy. Moreover, HRXRD does not confirm BZO presence due to either peak overlapping or because BZO are not aligned with (001)YBCO and a $\theta - 2\theta$ allows to acquire the full intensity of epitaxial phases.

Therefore, a first YBCO and secondary phases peak identification was done through GADDS. Fig.3(a) proves *c*-axis epitaxy as the scan exemplifies a standard four-fold symmetry YBCO sample. $\theta - 2\theta$ scans at different χ values confirmed the presence of BZO in YBCO-BZO films Fig.3(b) and Fig.3(c), where (011)BZO and (200)BZO peaks are identified. Notice that the BZO reflections (Fig.3(b), Fig.3(c)) are not indicating a ring, thus, suggesting that the nanoparticles might have a relevant degree of epitaxy. Although this is the typical case for YBCO nanocomposites growth from physical methods, it was never observed in CSD, except for the new TLAG process [6].

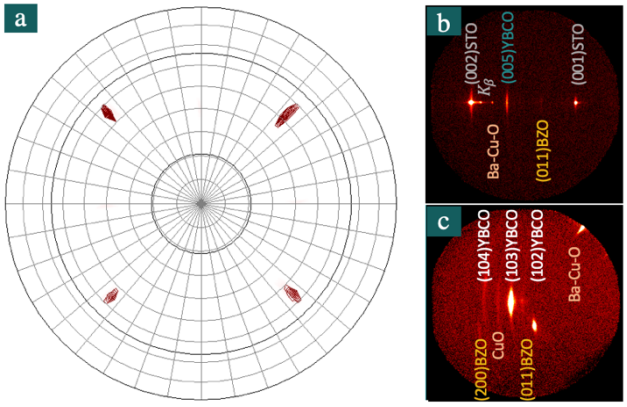

FIG. 3: XRD Structural characterization of two thin films grown at 827ºC, a pristine and a YBCO-BZO 24% mol. a) (104) Pole figure of YBCO pristine. b) $\theta - 2\theta$ two-dimensional pattern recorded for 1200s using GADDS of YBCO-BZO 24%mol measurement. The x-axis corresponds to $\theta - 2\theta$ and the rings to χ which varies with constant 2θ. Bragg peaks of STO, BZO and YBCO are identified. c) $\theta - 2\theta$ scan centred in $\chi = 45º$ recorded for 3600s using GADDS of YBCO-BZO 24%mol.

Once epitaxy and BZO presence were confirmed, a further microstructural analysis through Fig.2 was carried out. As Fig.4 shows, high epitaxial fractions were found in eleven out of fifteen samples. For the epitaxial samples, both rocking curve and nanostrains were obtained versus epitaxy degree. In Fig.4, the rocking curves indicate lower degree of out-of-plane texture for YBCO-BZO films (proportional to %mol of BZO)

than for pristine films, consistent with the growth disturbances induced in nanocomposites. This factor may be also related to the actual supersaturation conditions for each case, a key parameter of the growth process; lower supersaturation, may induce lower rocking curve.

Overall, the films' disorder degree is too low from both pristine and YBCO-BZO to interfere with the physical properties of the films, expected for misorientation angles of 1-4º.

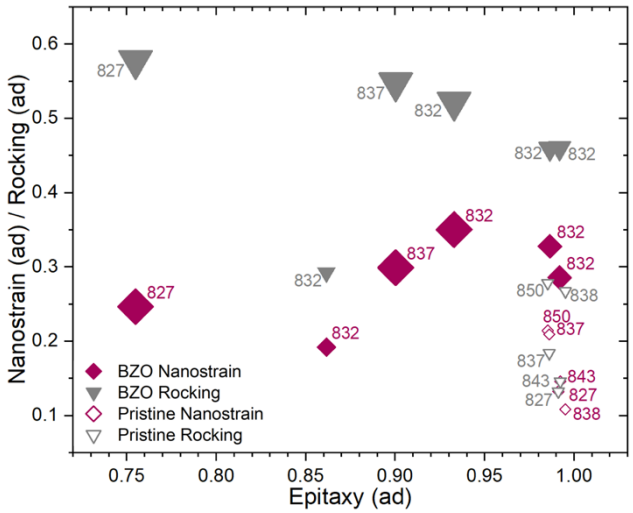

FIG. 4: Nanostrain and rocking versus epitaxy degree of eleven out of the fifteen samples, pristine and containing BZO. Growth temperature is indicated next to each dot, also YBCO-BZO dot size is proportional to the concentration of nanoparticles per mol: 0%, 6%, 12%, 24%. Error bars are smaller than the dot size in all cases.

Fig.4 shows for YBCO-BZO larger nanostrain values than pristine films. Although the BZO percentage does not seems to be a determinant factor to nanostrain contribution, as 24%mol BZO nanostrains are lower than 12%mol BZO. Further insights on this should be proved by TEM analysis.

B. Physical properties

As mentioned earlier, SQUID measurements were done to determine the critical current of the thin films, J_c. The SQUID self-field $J_c^{sf} = J_c(H = 0\,T)$, measurements at 5K, far from the irreversibility curve that marks the end of the superconductive properties, were promising at T_{growth} 827ºC both for the YBCO pristine film, $J_c^{pristine} = 19.94\ MA\ cm^{-2}$ and the YBCO-BZO 24%mol, $J_c^{827\_24BZO} = 1.77\ MA\ cm^{-2}$. However, it showed a rather poor performance for T_{growth} 832ºC YBCO-BZO 6%mol with $J_c^{832\_6BZO} = 0.277\ MA\ cm^{-2}$ and for T_{growth} 832ºC YBCO-BZO 12%mol $J_c^{832\_12BZO} \approx 3\ 10^{-4}\ MA\ cm^{-2}$. For YBCO-BZO 24%mol at T_{growth} 832ºC a $J_c^{832\_24BZO} = 1.24\ MA\ cm^{-2}$ and at T_{growth} 837ºC with $J_c^{837\_24BZO} = 1.05\ MA\ cm^{-2}$ performances were also obtained.

Notice that higher epitaxy and nanostrain values do not assure high J_c performance, as both T_{growth} 832ºC and T_{growth} 837ºC YBCO-BZO 24%mol films present higher epitaxy and nanostrain values, and achieve lower J_c performances than YBCO-BZO 24%mol at T_{growth} 827ºC. This suggests that current percolation is perturbed in some films. Even though their degree of epitaxy is high, the cross-section is reduced. Possible reasons might be an increase of porosity, bad distribution of secondary phases or agglomeration of some nanoparticles in nanocomposites (lower nanostrain). Additional measurements would be needed to calculate a more precise epitaxial rate. Moreover, the cross-section reduction is responsible for $J_c^{pristine} = 10 J_c^{827\_24BZO}$. Overall, it indicates that there is an optimum temperature where the peak of the superconducting performance is found.

A further comparison relating the pinning properties was made between $J_c^{pristine}$ and $J_c^{827\_24BZO}$ in Fig.5 by comparing their high magnetic fields dependence. The presence of BZO enhanced J_c in-field, as showed by Fig.5 inset, were H^*, which is a value proportional to the density of vortex pinning defects, is 7 times larger for BZO, H^*= 2109 mT, than for the pristine film, H^*= 923 mT. Moreover, $J_c^{pristine}$'s slope $(-0.4987 \pm 0.0009)\ MA\ cm^{-2}\ T^{-1}$ is lower compared with $J_c^{sf-827\_24BZO}$'s slope $(-0.572 \pm 0.005)\ MA\ cm^{-2}\ T^{-1}$ which indicates a much smoother magnetic dependence for the nanocomposite films, indicating a better vortex pinning behaviour. This behaviour proves that the defects are more effective for the BZO enhanced samples, which is consistent with the nanostrain and rocking values in Fig.4. In addition, these results suggest that the J_c values in nanocomposites are mediated by cross-section effects, that should be improved by further tunning the process parameters in order to avoid secondary phases inside the films.

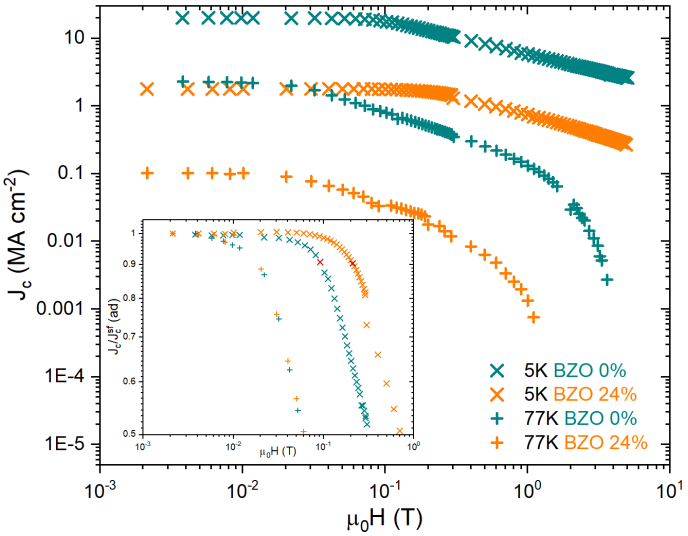

FIG. 5: Critical current density, J_c as a function of the magnetic field J (H ∥ c) for a TLAG pristine film and YBCO-BZO 24%mol both grown at 827ºC at 5K and 77K. Inset: J_c normalized with J_c^{sf}.The H^* parameter mark in red, is defined as the H value at 0.9 times J_c at self-field.

J_c measurements at 77K are ten times lower than 5K values as expected, the difference is due to the cross-section. However, if compared 77K results J_c are nearly identical. A higher J_c^{sf} for the nanocomposites film should be obtained in order to disclose its advantages from a pristine layer [4].

PPMS was carried in both 827ºC grown films. A critical temperature (T_C) of (90.6 ± 0.4) K was found for the pristine film and of (89.2 ± 0.6) K for the YBCO-BZO 24%mol, where T_C is the mean value of the transition and the uncertainty value sets its temperature range, as can be observed in Fig.6. Both results are in agreement with literature as YBCO $T_C \sim 92$K [2]. The small decrease observed in the

nanocomposites case could be due to the strained regions between the YBCO matrix and the BZO epitaxial nanoparticles. However, further analysis should be carried out to confirm it.

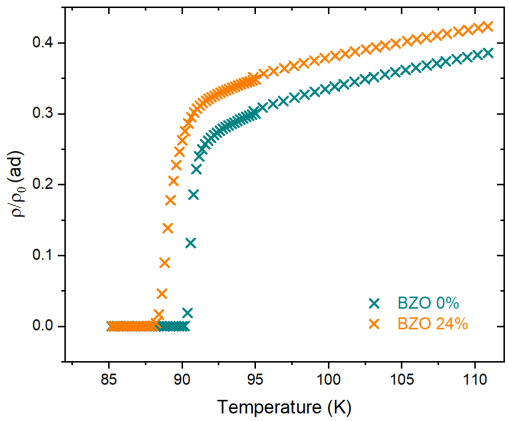

FIG.6: Resistivity versus temperature from transport measurements for a YBCO pristine and YBCO-BZO 24%mol grown at 827ºC.

V. INK-JET PRINTED SAMPLES

IJP has been proved to be a plausible deposition technique for thick pristine films [8] and also colloidal thin films [7]. However, the new combinational chemistry approach enables to control the desired amount of films' nanoparticles and landscape and consequently its lattice disorders. For this purpose, an algorithm was created in order to distribute homogeneously a BZO solution in a YBCO precursor wet film, specifically to distribute homogeneously the YBCO precursor and BZO nanoparticles solutions drops by printing the desired concentration of BZO. First experiments needed to overcome that the BZO-nanoparticles solution would not block the nozzle and the formulation of the solution had to be slightly modified by an amine additive.

Very recently, we have been able to start printing nanocomposites using this algorithm although the obtained results could not be thoroughly analysed yet.

VI. CONCLUSIONS

A new transient liquid assisted growth process was explored through the growth of fifteen spin-coated deposed samples, six YBCO and nine YBCO-BZO nanocomposite thin films. High *c*-axis epitaxial growth rates were found in eleven out of fifteen samples, higher for the pristine than the nanocomposite films, indicating that nanocomposites need more fine tuning of the process parameters than pristine films, probably by disturbances induced by the nanoparticles.

Nevertheless, superconducting performances were obtained at 5K up to 1.77 MA cm^{-2} for YBCO-BZO 24%mol at different growth temperatures, the best at 827ºC. YBCO-BZO nanocomposites show enhanced high magnetic field performance indicating better vortex pinning properties by higher density of artificial pinning centres consistent with higher H^* values. A critical temperature of (89.2 ± 0.6)K was obtained for YBCO-BZO 24%mol thin film and of (90.6 ± 0.4) K for a pristine film, both grown at T_{growth} = 827ºC.

Even though a further analysis could not be carried by for the inkjet printed films, the new combinational chemistry approach proves to be valid for YBCO-BZO nanocomposites printing. Hence, to future manufacturing of coated conductors.

Acknowledgments

I would like to thank my advisors from the SUMAN group at ICMAB-CSIC, Dr. Albert Queraltó and Prof. Teresa Puig for the trust, support, and opportunity to join their group within the Ultrasupertape ERC project. I also thank my UB advisor Prof. Arantxa Fraile Rodríguez for her guidance.

[1] X. Obradors and T. Puig, "Coated conductors for power applications: Materials challenges," *Supercond. Sci. Technol.*, vol. 27, no. 4, 2014.

[2] V. Breit *et al.*, "Evidence for chain superconductivity in near-stoichiometric YBa2Cu3Ox single crystals," *Phys. Rev. B.*, vol. 52 no. 22, pp. R15727–R15730, 1995.

[3] N. F. Heinig *et al.*, "Evidence for channel conduction in low misorientation angle [001] tilt YBa2Cu3O7- x bicrystal films," *Appl. Phys. Lett.*, vol. 69, no. 4, pp. 577–579, 1996.

[4] A. Llordés *et al.*, "Nanoscale strain-induced pair suppression as a vortex-pinning mechanism in high-temperature superconductors," *Nat. Mater.*, vol. 11, no. 4, pp. 329–336, 2012.

[5] S. Kang *et al.*, "High-Performance High-Tc Superconducting Wires," vol. 2083, no. March, pp. 1911–1915, 2006.

[6] L. Soler *et al.*, "Ultrafast transient liquid assisted growth of high current density superconducting films," *Nat. Commun,* 2020.

[7] I. Van Driessche *et al.*, "Chemical solution deposition using ink-jet printing for YBCO coated conductors," *Supercond. Sci. Technol.*, vol. 25, no. 6, 2012.

[8] C. Pop *et al.*, "Growth of all-chemical high critical current YBa 2 Cu 3 O 7-δ thick films and coated conductors," *Supercond. Sci. Technol.*, vol. 32, no. 1, 2019.

[9] L. Soler, "Liquid-assisted ultrafast growth of superconducting films derived from chemical solutions.," 2019.

[10] H. Rijckaert *et al.*, "Superconducting HfO2-YBa2Cu3O7−δ Nanocomposite Films Deposited Using Ink-Jet Printing of Colloidal Solutions," *Coatings*, vol. 10, no. 1, p. 17, 2019.

[11] C. P. Bean, "Magnetization of hard superconductors," *Phys. Rev. Lett.*, vol. 8, no.6, p. 250, 1962.

[12] L.J. Van der Pauw, "A method of measuring the resistivity and hall coeficient on lamellae of arbitrary shape," *Philips Tech. Rev.*, vol. 20, pp. 220–224, 1958.

[13] A. Queraltó, "Growth of functional oxide heterostructures from chemical solutions using advanced processing methodologies," 2015.